1521-009X/50/3/197–203$35.00
DRUG METABOLISM AND DISPOSITION

dx.doi.org/10.1124/dmd.121.000774
Drug Metab Dispos 50:197–203, March 2022

Comparison of Tissue Abundance of Non-Cytochrome P450 Drug-Metabolizing Enzymes by Quantitative Proteomics between Humans and Laboratory Animal Species[S]

Abdul Basit, Peter W. Fan, S. Cyrus Khojasteh, Bernard P. Murray, Bill J. Smith, Scott Heyward, and Bhagwat Prasad

Department of Pharmaceutical Sciences, Washington State University, Spokane, Washington (A.B., B.P.); Department of Pharmacokinetics, Pharmacodynamics, and Drug Metabolism, Merck & Co., Inc., Boston, Massachusetts (P.W.F.); Department of Drug Metabolism and Pharmacokinetics, Genentech Inc., South San Francisco, California (S.C.K.); Drug Metabolism and Pharmacokinetics Department, Gilead Sciences Inc., Foster City, California (B.P.M., B.J.S.); and BioIVT Inc., Baltimore, Maryland (S.H.)

Received November 10, 2021; accepted December 13, 2021

ABSTRACT

The use of animal pharmacokinetic models as surrogates for humans relies on the assumption that the drug disposition mechanisms are similar between preclinical species and humans. However, significant cross-species differences exist in the tissue distribution and protein abundance of drug-metabolizing enzymes (DMEs) and transporters. We quantified non–cytochrome P450 (non-CYP) DMEs across commonly used preclinical species (cynomolgus and rhesus monkeys, beagle dog, Sprague Dawley and Wistar Han rats, and CD1 mouse) and compared these data with previously obtained human data. Aldehyde oxidase was abundant in humans and monkeys while poorly expressed in rodents, and not expressed in dogs. Carboxylesterase (CES) 1 abundance was highest in the liver while CES2 was primarily expressed in the intestine in all species with notable species differences. For example, hepatic CES1 was 3× higher in humans than in monkeys, but hepatic CES2 was 3–5× higher in monkeys than in humans. Hepatic UDP-glucuronosyltransferase (UGT) 1A2 abundance was ~4× higher in dogs compared with rats, whereas UGT1A3 abundance was 3–5× higher in dog livers than its ortholog in human and monkey livers. UGT1A6 abundance was 5–6× higher in human livers compared with monkey and dog livers. Hepatic sulfotransferase 1B1 abundance was 5–7× higher in rats compared with the rest of the species. These quantitative non-CYP proteomics data can be used to explain unique toxicological profiles across species and can be integrated into physiologically based pharmacokinetic models for the mechanistic explanation of pharmacokinetics and tissue distribution of xenobiotics in animal species.

SIGNIFICANCE STATEMENT

We characterized the quantitative differences in non–cytochrome P450 (non-CYP) drug-metabolizing enzymes across commonly used preclinical species (cynomolgus and rhesus monkeys, beagle dogs, Sprague Dawley and Wistar Han rats, and CD1 mice) and compared these data with previously obtained human data. Unique differences in non-CYP enzymes across species were observed, which can be used to explain significant pharmacokinetic and toxicokinetic differences between experimental animals and humans.

Introduction

Preclinical models are an integral part of the drug discovery and development process. Despite advanced in vitro models, preclinical pharmacokinetics (PK) and toxicity data conducted in laboratory animal species make up the foundation of investigational new drug applications (Barre-Sinoussi and Montagutelli, 2015). Moreover, exploratory tissue distribution studies can only be performed in preclinical species. The commonly used preclinical species in drug testing are mice (CD1), rats (Sprague Dawley and Wistar Han), dogs (beagle), and nonhuman primates (cynomolgus and rhesus). These preclinical models have several advantages: 1) they represent complete physiologic systems for absorption, distribution, metabolism, and excretion processes, 2) both PK and pharmacodynamics can be studied simultaneously, and 3) they present fewer ethical hurdles as compared with clinical studies (Barre-Sinoussi and Montagutelli, 2015). However, animal studies are often associated with limitations of interspecies differences in the processes that govern absorption, distribution, metabolism, and excretion processes and pharmacodynamics.

With respect to drug disposition, experimental animals are significantly different from humans. While monkeys are genetically the closest species to humans, both protein abundance and substrate affinity (Km) to enzymes and transporters can be largely different between humans and monkeys. An antiviral agent, favipiravir, which is converted into the inactive oxidative metabolite mainly by aldehyde oxidase (AOX),

This work was funded by the Proteomics-based Research Initiative for Non-CYP Enzymes (PRINCE) consortium: Genentech Inc., Gilead Sciences Inc., and Merck & Co., Inc.

The authors declare that they have no conflicts of interest with the contents of this article.

dx.doi.org/10.1124/dmd.121.000774.

[S] This article has supplemental material available at dmd.aspetjournals.org.

ABBREVIATIONS: ABC, ammonium bicarbonate; AOX, aldehyde oxidase; BSA, bovine serum albumin; CES, carboxylesterase; DME, drug-metabolizing enzyme; Km, substrate affinity; Non-CYP, non–cytochrome P450; PK, pharmacokinetics; SULT, sulfotransferase; UGT, UDP-glucuronosyltransferase.

shows large interspecies differences in its metabolism, with the highest metabolic clearance in monkeys, followed by humans, mice, and finally rats (Hanioka et al., 2021). The abundance of organic anion transporter 1, organic cation/carnitine transporter 2 (OCTN2), and multidrug resistance–associated protein 4 in kidney tissues is ∼3× higher in monkeys than humans (Basit et al., 2019). The abundance of multidrug resistance protein, or P-glycoprotein, is higher in male versus female kidneys in rats, whereas its abundance in mouse kidneys is significantly higher in females than males (Basit et al., 2019). Therefore, it is important that the abundance and activity of enzymes and transporters are characterized across species. While cross-species data are available on transporters and CYPs (Wang et al., 2015; Basit et al., 2019; Hammer et al., 2021), protein abundance data for non-CYP enzymes are lacking, which is often associated with the uncertainty in predicting human PK and toxicity of investigational drugs. A notable example is the unpredictable nephrotoxicity associated with an insoluble AOX metabolite, 2-quinolinone-SGX523, in humans (Diamond et al., 2010). Insufficient efflux of this metabolite is the likely cause of its accumulation in human kidneys, leading to nephrotoxicity that can be explained by differences in the protein abundance, as well as the substrate affinity to the transporters in the kidney. Variable rates of hydrolysis of clopidogrel to its inactive but major metabolite, clopidogrel carboxylic acid, across species highlight the species difference in carboxylesterase (CES) 1–mediated hydrolysis. In particular, the formation rate of clopidogrel carboxylic acid was slowest in rats and fastest in minipigs (Wang et al., 2020). This variability in hydrolysis of prodrug across species might complicate the dose extrapolation from one species to another and may lead to either loss of efficacy or higher exposure associated with adverse events (Wang et al., 2020).

The lack of specific probe substrates, inhibitors, and in vitro models to study non-CYP enzymes is another critical challenge. Further, knowledge gaps with respect to the extrahepatic abundance of non-CYP enzymes adds additional challenges in predicting their roles in drug metabolism and toxicity. Further, non-CYP metabolites formed by CESs and AOX are often associated with secondary metabolism, which can become rate-limiting in the elimination of the primary metabolites from tissues. In such cases, it is essential to understand the critical rate limiting steps of primary metabolism that affect the drug clearance and tissue exposure. Since the metabolism of drugs often involves sequential processes (e.g., Phase I and Phase II metabolism), species differences in enzyme abundance can affect metabolite profiles in experimental animals versus humans. For example, irinotecan metabolism to SN-38 by CES2 is rate-limiting for hepatic SN-38 exposure, whereas UDP-glucuronosyltransferase (UGT) 1A1 is the rate-limiting step for intestinal SN-38 exposure (Parvez et al., 2021). Therefore, it is important to characterize the relative abundance of sequential enzyme systems such as CESs and UGTs. Considering these challenges, we quantified interspecies differences in protein abundance of AOX, CESs, UGTs, and sulfotransferases (SULTs) as a first step toward better interpretation and scaling of preclinical data to human.

Materials and Methods

Materials. Methanol, mass spectrometry (MS)-grade acetonitrile, and formic acid were purchased from Fisher Scientific (Fair Lawn, NJ). Acetone was purchased from Sigma-Aldrich (St. Louis, MO). Bicinchoninic acid kit for total protein quantification was purchased from Pierce Biotechnology (Rockford, IL). Ammonium bicarbonate (ABC) (98% pure), dithiothreitol, iodoacetamide, and trypsin were procured from Thermo Fisher Scientific (Rockford, IL). Human serum albumin and bovine serum albumin (BSA) were purchased from Calbiochem (Billerica, MA) and Thermo Fisher Scientific (Rockford, IL), respectively. Synthetic unlabeled peptides with amino acid analysis and stable labeled (heavy) peptides were purchased from New England Peptides (Boston, MA) and Thermo Fisher Scientific (Rockford, IL), respectively.

Procurement of Tissue Samples from Preclinical Species and Collection of Human Data. Unless otherwise stated here, tissue homogenate samples from preclinical species were provided by BioIVT Inc. (Baltimore, MD). Pooled Sprague Dawley rat intestinal S9 (n = 200), Wistar Han rat liver S9 (n = 240), and rhesus monkey pooled liver S9 (n = 6) and intestinal S9 (n = 7) fractions were procured from SEKISUI Xenotech (Kansas City, KS). The human data were obtained from our previous study (Basit et al., 2020), for which the demographic information is provided in Supplemental Table 1. The details of the preclinical samples are provided in Table 1.

TABLE 1

Characteristics and source of tissues from preclinical species

Species	Tissue	Donor (n)	Sex	Pooled/Individual	Source
CD1 mouse	Liver	12	M	Pooled	BioIVT
	Kidney	12	M	Pooled	BioIVT
	Intestine	12	M	Pooled	BioIVT
	Heart	12	M	Pooled	BioIVT
SD Rat	Liver	6	M	Pooled	BioIVT
	Kidney	6	M	Pooled	BioIVT
	Intestine	200	M	Pooled	SEKISUI XenoTech
	Heart	6	M	Pooled	BioIVT
WH Rat	Liver	240	M	Pooled	SEKISUI XenoTech
	Kidney	6	M	Pooled	BioIVT
	Intestine	6	M	Pooled	BioIVT
	Heart	6	M	Pooled	BioIVT
Beagle Dog	Liver	3	2 M, 1 F	Individual	BioIVT
	Kidney	3	M	Individual	BioIVT
	Intestine	3	M	Individual	BioIVT
	Heart	3	M	Individual	BioIVT
Cynomolgus	Liver	4	M	Individual	BioIVT
	Kidney	3	M	Individual	BioIVT
	Intestine	4	M	Individual	BioIVT
	Heart	1	M	Individual	BioIVT
Rhesus	Liver	6	M	Pooled	SEKISUI XenoTech
	Intestine	7	M	Pooled	SEKISUI XenoTech
Human[a]	Liver	21	12 M, 9 F	Individual	University of Washington
	Kidney	22	13 M, 9 F	Individual	University of Washington
	Intestine	14	10 M, 4 F	Individual	BioIVT
	Heart	17	10 M, 7 F	Individual	University of Washington

[a]Previously analyzed human data were used to compare cross-species differences in DME abundance.

S9 Subcellular Preparation. S9 fractions were prepared from tissue homogenates as described previously (Prasad et al., 2018). Briefly, the homogenate was centrifuged at 9000*g* for 30 minutes at 4°C. The supernatant (S9 fraction) was transferred to a new 1.5 mL centrifuge tube. Total protein in tissue samples was quantified using the bicinchoninic acid assay kit (Pierce Biotechnology, Rockford, IL) following the vendor protocol. S9 fractions were stored at −80°C prior to liquid chromatography tandem mass spectrometry (LC-MS/MS) analysis.

Surrogate Peptide Selection Strategy. Selection of surrogate peptides is the first critical step in targeted proteomics quantification by LC-MS/MS. A detailed list of criteria for selection of signature peptides is described previously (Bhatt and Prasad, 2018) and presented in Supplemental Figure 1. In brief, an ideal peptide should be unique, sensitive, stable, soluble, and LC-MS–compatible. Surrogate peptides should be unique to the protein of interest in a particular species, which can be confirmed by protein sequence homology search, such as by using Protein Prospector (http://prospector.ucsf.edu/prospector/mshome.htm). In addition, we selected the surrogate peptides that are orthologous in at least one more species to allow quantification using a matrix approach (Basit et al., 2019). However, in cases where orthologous peptides were not available, we selected peptides with only 1–3 amino acid differences and retained terminal amino acids to avoid variability in response (Supplemental Table 2).

Sample Preparation and LC-MS/MS Analysis of Targeted Peptides. The S9 samples were digested using a previously optimized protocol (Ahire et al., 2021). Briefly, 80 µL of S9 sample (1 mg/mL total protein) was mixed with 30 µL ABC (100 mM), and 20 µL of BSA (0.02 mg/mL) in a 1.5-mL microcentrifuge tube. The proteins were denatured and reduced with 10 µL 250 mM dithiothreitol at 95°C for 10 minutes with gentle shaking at 300 rpm. The sample was cooled to room temperature for 10 minutes, and the denatured proteins were alkylated with 10 µL of 500 mM iodoacetamide in the dark for 30 minutes. Ice-cold acetone (1 mL) was added to precipitate proteins, followed by vortex mixing and centrifugation at 16,000*g* (4°C) for 5 minutes. The supernatant was removed using vacuum suction. The protein pellet was dried for 10 minutes at room temperature and washed with 500 µL ice-cold methanol, followed by centrifugation at 8000*g* (4°C) for 5 minutes. The supernatant was removed, and the pellet was dried at room temperature for 30 minutes and resuspended in 60 µL ABC buffer (50 mM, pH 7.8). Finally, the resuspended protein sample was digested by adding 20 µL of trypsin (protein: trypsin ratio, ~25:1) and incubated at 37°C for 16 hours. The reaction was quenched by the addition of 20 µL of the peptide internal standard cocktail (prepared in 40% acetonitrile in water containing 0.5% formic acid) and 10 µL 1% formic acid in water. The sample was vortex mixed and centrifuged at 4000*g* for 5 minutes. The supernatant was collected in an LC-MS vial for analysis.

The samples were analyzed using an M-class Waters UPLC system coupled with a Waters Xevo TQ-XS µLC-MS/MS instrument supported by IonKey interphase. The peptides were separated on an iKey HSS T3 C18 column (130 Å, 1.8 µm, 150 µm × 150 mm) and nano-Ease Symmetry C18 trap column (300 µm × 50 mm) (Waters, Milford, MA). The optimized µLC-MS/MS acquisition parameters are provided in Supplemental Table 3.

Data Analysis. The LC-MS/MS data were analyzed using Skyline 19.1 (University of Washington, Seattle, WA). Briefly, the peptide peaks were identified by matching the retention time with the heavy internal standards and alignment of the selected precursor ion to the respective product ion fragments. A previously optimized robust data analysis approach was used (Wang et al., 2021), which considers the internal standard protein (BSA), heavy internal standard peptide, and previously characterized pooled sample. The absolute protein abundance (pmol/mg protein) was performed by using a previously characterized pooled sample as the calibrator (Bhatt and Prasad, 2018). Protein abundance data across human tissues were compared using the Kruskal-Wallis test, followed by Dunn′s multiple comparison test (across three or more groups) and the Mann-Whitney test (between two groups).

Results

In this study, we quantified non-CYP DMEs in humans and four commonly used preclinical animal models, i.e., nonhuman primates (cynomolgus and rhesus monkeys), beagle dogs, Wistar Han and Sprague Dawley rats, and CD-1 mice across four tissues (liver, intestine, kidney, and heart). These data were compared with our previously generated protein abundance data for human non-CYP DMEs (AOX1, CESs, SULTs, and UGTs) (Basit et al., 2020). Wherever the surrogate peptide is conserved in preclinical species and humans, we reported absolute DME abundance data in picomoles per milligrams of protein, otherwise, relative abundance data (normalized to total protein) are presented.

Protein Sequence Similarity Between Human and Preclinical Species and Peptide Selection for Selective Quantification. We used UniProt (https://www.uniprot.org/) and US National Center for Biotechnology Information's basic local alignment search tool (BLAST; https://blast.ncbi.nlm.nih.gov/) to compare the sequence similarity between proteins in humans and preclinical species. As shown in Fig. 1 and Supplemental Table 4, humans and monkeys are similar in their protein sequences, with greater than 90% sequence similarity across proteins, except for CES2 in cynomolgus monkey. In dogs, rats, and mice, non-CYP enzymes showed 60–80% sequence similarity for AOX, CES, and SULTs. Although there are four mammalian isoforms of AOX (AOX1–4), differences exist in the expression of these genes between human and preclinical species. Mice and rats express four distinct AOX proteins, dogs and monkeys express two AOX isoforms, and humans have only one isoform (Manevski et al., 2019). Table 2 presents

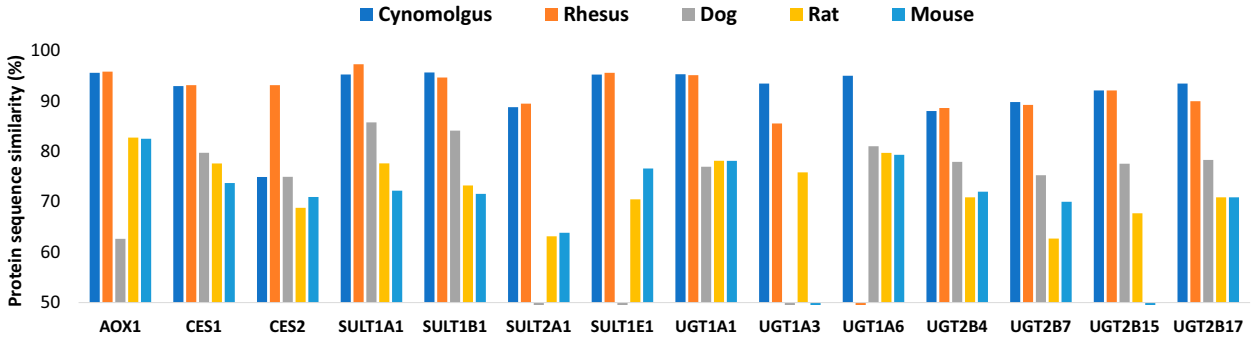

Fig. 1. Protein sequence similarity (%) of various non-CYP enzymes between human and preclinical species. The nomenclature of AOX and UGTs is not consistent across species. Dogs do not express AOX1, therefore AOX2 was quantified in dogs as it showed >60% sequence similarity with human AOX1. Human UGT1A3 has the closest sequence similarity to UGT1A4 in cynomolgus monkeys (93%). Human UGT2B4 has closet sequence similarity to UGT2B19 or 2B30 in monkeys (88%), UGT2B31 in dogs (78%), UGT2B31, or UGT2B10 in rats (71%). Human UGT2B7 has closest sequence similarity to UGT2B9 or UGT2B18 in cynomolgus monkeys (90%), UGT2B31 in dogs (75%), and UGT2B4 or UGT2B10 in mice (70%). Human UGT2B15 has the closest sequence similarity to UGT2B20 in rhesus monkeys (92%) and UGT2B31 in dogs (76%). Human UGT2B17 has closest sequence similarity to UGT1A4a in cynomolgus monkeys (93%), UGT2B20 in rhesus monkeys (90%), UGT2B31 in dogs (78%), UGT2B1 in rats (71%), and UGT2B4 in mice (71%). Details are provided in Supplemental Table 4.

TABLE 2

Reported data on the localization of AOX isoforms in preclinical species and human
Unknown indicates that the protein is expressed, but the localization is not characterized.

Protein	Tissue(s)				
	Mouse	Rat	Dog	Monkey	Human
AOX1	Liver, esophagus, lung, heart, Harderian gland, olfactory mucosa, skin, testis, brain, spinal cord, and eye	Liver, heart, lung, spleen, and kidney	NP	Liver, lung, kidney, lacrimal gland, and olfactory mucosa	Liver, adipose tissue, lung, skeletal muscle, and pancreas
AOX2	Olfactory mucosa epithelium and skin	Unknown	Thyroid gland	Nasal mucosa	NP
AOX3	Liver	Unknown	NP	NP	NP
AOX4	Harderian gland, sebaceous gland, epidermis, and testis	Harderian gland, sebaceous gland, epidermis, and testis	Nose, mammary gland, skin, testis, and brain	NP	NP

NP, gene or protein not present.

the tissue localization of various AOX isoforms in humans, monkeys, dogs, rats, and mice. Moreover, as shown in Fig. 1, AOX1 is the only hepatic isoform in humans, monkeys, and rats, although mouse AOX3 is also localized in the liver. Localization of dog AOX proteins is not well characterized. We only quantified AOX1 or its analogous isoforms because humans and most primates contain a single active AOX gene—AOX1—which has the highest sequence similarity with mouse and rat AOX1. Because dogs do not express AOX1, we quantified AOX2 in dogs, as it shows >60% sequence similarity with human AOX1.

UGT protein sequences were challenging to compare due to the differences in their nomenclature. For example, UGT2B7 in humans is 89% similar to UGT2B9 or UGT2B18 in cynomolgus monkeys. This poses a challenge in surrogate peptide selection. Therefore, we relied on quantitative proteomics analysis of unique species-specific surrogate peptides for UGT isoforms (Supplemental Table 2).

Absolute Abundance of Non-CYP Enzymes in Human and Nonhuman Primates. Nonhuman primates share higher similarity in protein sequence (Table 2), hence it was possible to identify the conserved signature peptides between human and nonhuman primates (except for UGTs) to quantify and compare the abundance of non-CYP enzymes in humans and nonhuman primates. In general, AOX is highly abundant in the liver compared with other tissues. Hepatic AOX abundance in monkeys was comparable to that in humans (~1.6× difference) (Fig. 2). In the intestine, AOX is 2.2× higher in cynomolgus monkeys compared with rhesus monkeys, but it is not detectable in the human intestine. Hepatic CES1 abundance was 3× higher in humans compared with nonhuman primates. In contrast, intestinal and kidney abundance in nonhuman primates are 20–40× higher than in humans. Similarly, CES2 abundance is higher in nonhuman primate intestines than in human intestines. In nonhuman primates, ~2× higher abundance of CES2 was observed in the liver as compared with the intestine. In general, SULT1A1 levels are 3–5× higher in both intestines and livers

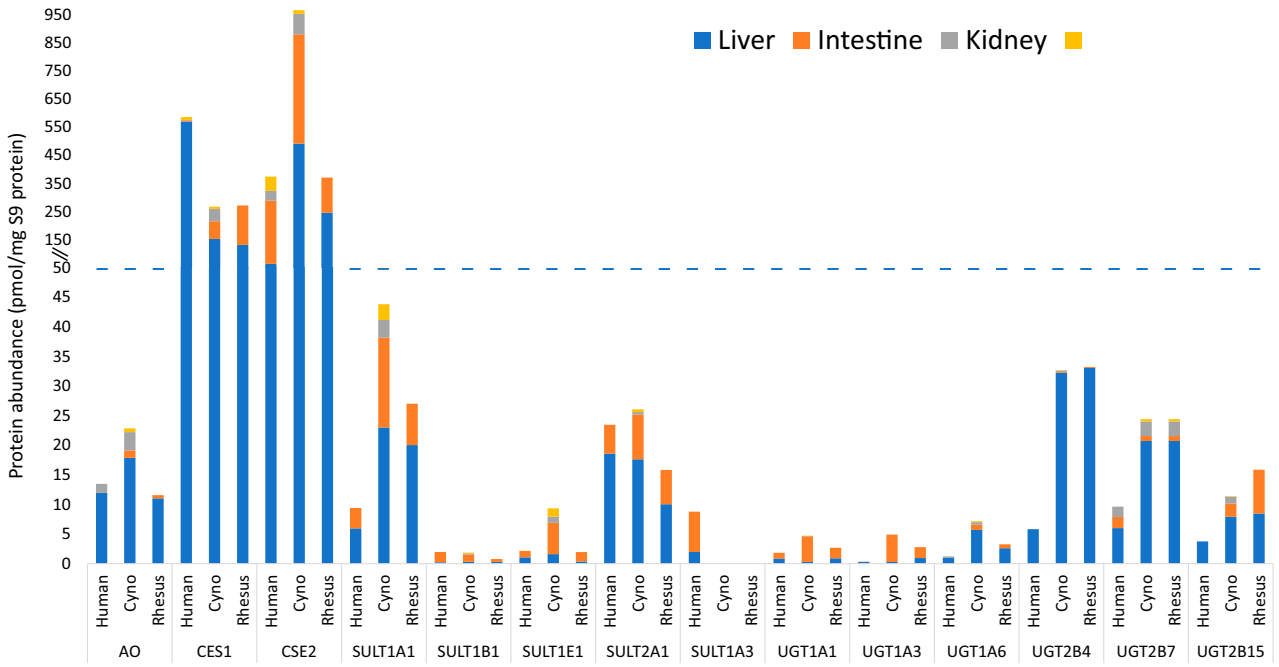

Fig. 2. Comparison of absolute abundance (pmol/mg S9 protein) of non-CYP enzymes in humans and monkeys across tissues. The data are presented for the proteins sharing conserved peptides between humans and monkeys.

of the nonhuman primates compared with corresponding human tissues. Interestingly, SULT1A1 was detected in the kidney of cynomolgus monkeys, but it was below the limit of quantification in human kidneys. Similarly, SULT1B1 and SULT2A1 were also observed in the cynomolgus kidney, and they were similar in the liver and the intestine between humans and the nonhuman primates. Regarding UGTs, the levels of UGT1A1 between the intestine and liver were similar in humans, while 2–12× higher intestinal abundance of UGT1A1 was detected in the nonhuman primates. Hepatic abundance of UGT1A6 was 2–5× higher in the nonhuman primates compared with humans. UGT1A6 was also detected in the monkey intestines and kidneys. Hepatic UGT2B4 and UGT2B7 were 6× and >3× higher, respectively, in the nonhuman primates compared with humans. In the intestines and kidneys, UGT2B7 levels were comparable between humans and the nonhuman primates. While UGT2B15 was below the limit of quantification in the human intestine, the nonhuman primates showed comparable levels of UGT2B15 in the liver and the intestine.

Hepatic Abundance of Non-CYP Enzymes Across Species. The majority of non-CYP enzymes were predominantly detected in the livers across all the species (Fig. 3). AOX1 is not expressed in dogs and poorly expressed in rodents, however its abundance is 3–5× higher in rats as compared with mice. Hepatic CES1 is 3× higher in humans than in monkeys, but CES2 is 3–5× higher in nonhuman primates than in humans. Hepatic CES2 abundance is 3–10× lower in rodents than in humans and monkeys. SULT1A1 abundance in the liver is 4×, 7×, 5×, and 3× higher in the nonhuman primates, dogs, and rats, respectively, than in humans, whereas it was 2× lower in mice. SULT1B1 abundance is comparable in human and nonhuman primate livers, whereas it is 5–7× higher in rats compared with the other species tested. Hepatic UGT1A2 expression is ∼4× higher in dogs than in rats. UGT1A3 abundance is 3–5× higher in dog livers than in human and monkey livers. UGT1A6 abundance in the liver is 5–6× higher in humans compared with monkeys and dogs.

Relative Extrahepatic to Hepatic Abundance on Non-CYP Enzymes across Species. AOX is predominantly expressed in the liver in all tested species with a measurable expression in kidneys (human and monkey) and intestine (monkey). (Fig. 4). CES1 expression is higher in the liver, whereas CES2 is predominant in the intestine in all the tested species. UGT1A1, UGT1A2, UGT1A3, UGT1A7, UGT2B17, and UGT2B34 were highly expressed in the intestine, whereas UGT1A6, UGT2B4, UGT2B7, UGT2B9, UGT2B15, and UGT2B35 were predominantly detected in the liver. SULT1B1, SULT1E1, and SULT1A3 expression was higher in the intestine than in the liver. The ratio of enzyme abundance between tissues showed high interspecies variability. The intestine-to-liver ratio of CES2 abundance was 4 (human), 1 (cynomolgus), 1 (rhesus), 15 (dog), and 20 (rat). While SULT1A1 intestine-to-liver ratio was similar across humans, monkeys, and dogs, it was uniquely expressed in dog kidneys (1.5× higher than in livers). The intestine-to-liver ratio of SULT1B1 was 8 (human), 5 (cynomolgus), 2 (rhesus monkey), and 35 (dog). The intestine-to-liver ratio of SULT2A1 and SULT1E1 showed a similar pattern, with a 2–4× higher ratio in monkeys than in humans. Although the intestine-to-liver ratio for UGT1A1 in humans was 1, the ratio was higher in preclinical species, i.e., 14 (cynomolgus and rhesus monkey), 2.5 (rat), and 1.2 (mouse).

Discussion

Animal-to-human scaling of PK and toxicity data are important for the safety of healthy volunteers or patients, as well as to address the high attrition rate in clinical development. However, there are several examples where interspecies differences in drug disposition partly contributed to the discontinuation of clinical candidates (Semino-Mora et al., 1997; Attarwala, 2010). Such incidences are common if an investigational drug is an AOX substrate. For example, both SGX523 and JNJ-38877605 (Lolkema et al., 2015) were responsible for nephrotoxicity due to the formation of insoluble metabolites mediated by AOX in human kidneys, which ultimately led to their discontinuation as clinical candidates. Capmatinib, a highly selective and potent MET (tyrosine kinase receptor) inhibitor also failed due to high interspecies differences in its AOX-mediated metabolism and toxicity (Lolkema et al., 2015; Glaenzel et al., 2020). Considering the implications of interspecies differences in drug development, here we provided a quantitative comparison of non-CYP enzymes in humans versus nonhuman primates (cynomolgus and rhesus), dogs, rats, and mice. Our results showed large differences in both the cross-species abundance within one organ and the relative localization of these enzymes across different tissues.

Our data correlate with interspecies differences in the PK of drugs, and may potentially explain drug toxicity. For example, as discussed above, SGX-523 showed renal toxicity in humans, despite toxicology experiments performed in rodents and dogs, because it is metabolized by AOX to 2-quinolinone-SGX-523, which is accumulated in the human kidney. The high expression of AOX in humans and nonhuman primates compared with rodents and dogs, as shown in this study, is the

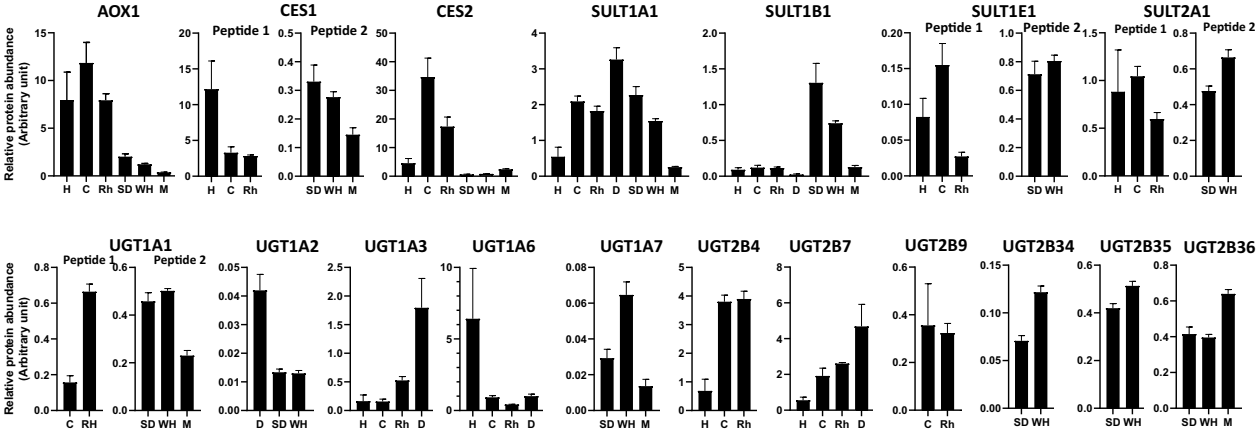

Fig. 3. Relative hepatic abundance (per mg of S9 protein) of non-CYP DMEs across species. X-axes represent the species (H, human; C, cynomolgus monkey; RH, rhesus monkey; D, beagle dog; SD, Sprague Dawley rat; WH, Wistar Han rat; M, CD1 mouse). Y-axes represent the relative protein abundance per mg protein. Supplemental Table 5 contains absolute abundance data for proteins where the peptide calibrators are available.

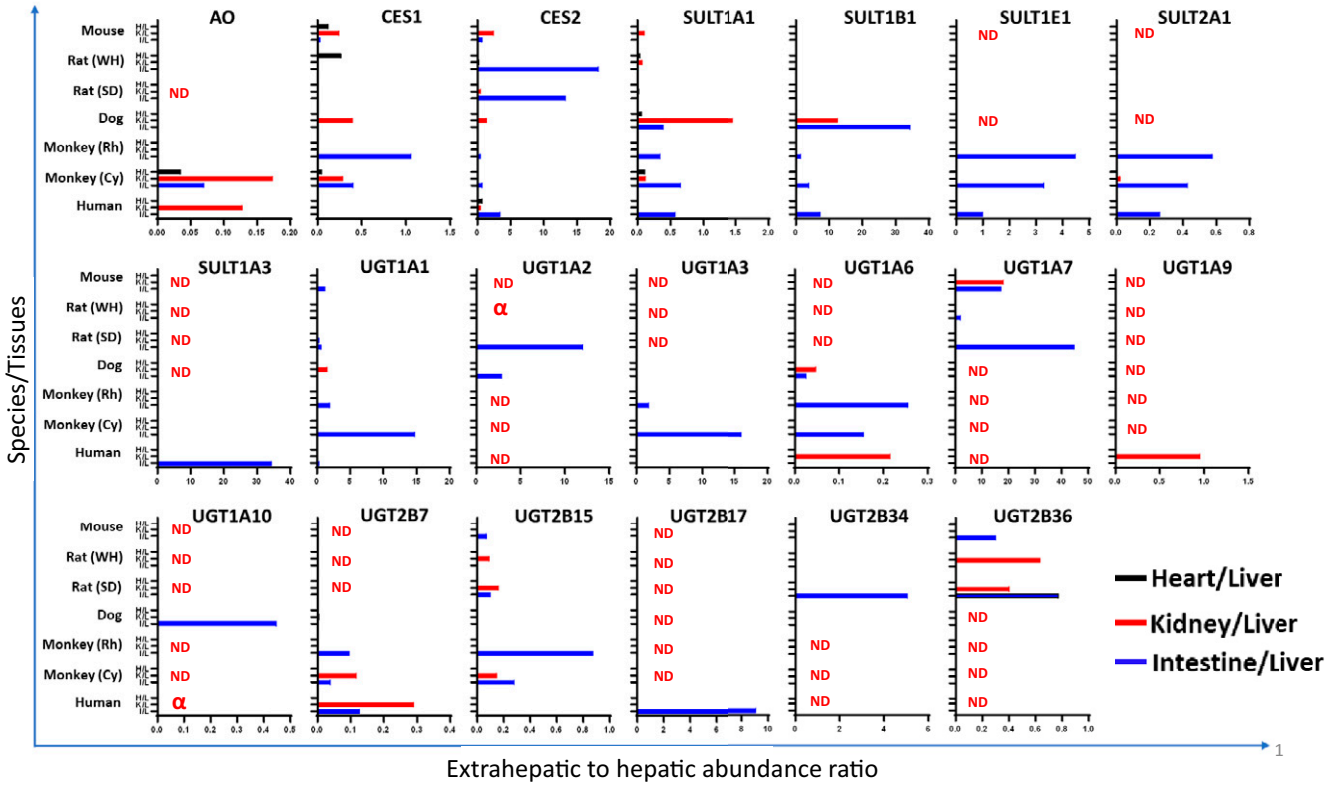

Fig. 4. Extrahepatic-to-hepatic abundance ratio for non-CYP DMEs across species. ND, not detected due to nonconserved isoform; α = intestinal-specific abundance.

likely reason for the toxic levels of the metabolite (Diao and Huestis, 2019). Similarly, a novel EGFR inhibitor, BIBX1382, failed in drug development because of poor oral bioavailability associated with its extensive AOX-mediated metabolism in humans compared with rodents (Uehara et al., 2021). Intestinal toxicity of irinotecan can also be explained by the tissue proteomics data presented here. Irinotecan is converted to active metabolite SN-38 via CES2 and then subsequently glucuronidated by UGT1A1 (Parvez et al., 2021) and both CES2 and UGT1A1 abundance play important roles in the intestinal toxicity. Our data suggest 3.5× higher abundance of CES2 in the intestine as compared with the liver, leading to the high local concentration of SN38 in the human intestine (Parvez et al., 2021). Since CES2 and UGT abundances are significantly different across species and organs, the differences in tissue-specific metabolism in human versus preclinical species may be associated with unexpected tissue metabolite profile and toxicity in humans. For example, the intestine-to-liver ratio of CES2 abundance in rats is higher than in humans, suggesting that irinotecan-to-SN38 conversion in relation to liver is faster in rats as compared

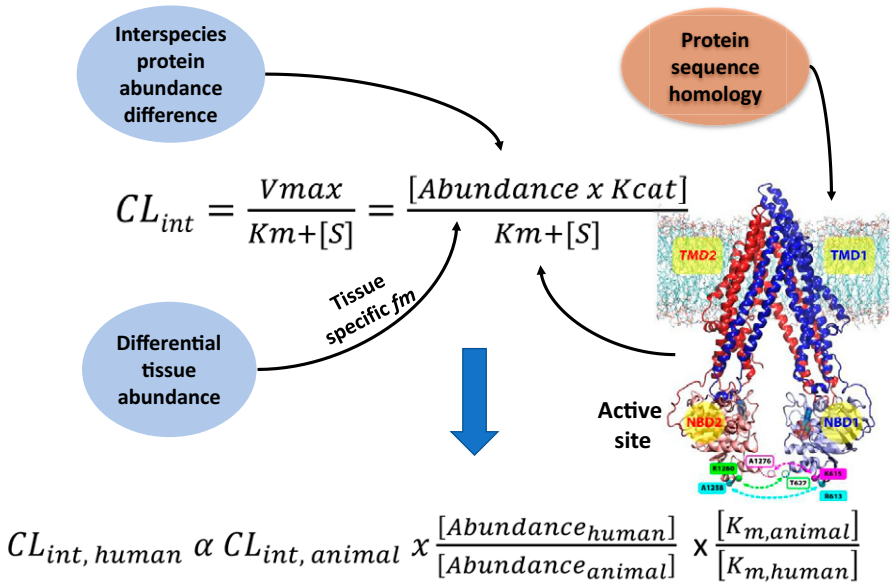

Fig. 5. Factors affecting interspecies extrapolation of non-CYP drug metabolism.

with humans (Fig. 4). Similarly, the prodrugs that are hydrolyzed in the intestine by CES enzymes such as dabigatran etexilate, olmesartan, methylphenidate, and temocapril (Di, 2019) would experience variable hydrolysis between species.

The interspecies differences in the abundance of non-CYP enzymes may not be directly used in scaling animal data to humans due to differences in the substrate affinity (Km) to individual proteins (Zou et al., 2018). We propose a systematic workflow that can be integrated into physiologically based pharmacokinetic modeling for quantitative scaling of non-CYP drug metabolism (Fig. 5). Here, if the recombinant proteins are available from multiple species, the potential isoforms involved in metabolism can be shortlisted, which can then be investigated to estimate Km and V_{max} values across species. Finally, the scaling would require normalization of the in vitro clearance data obtained in animal species with abundance, as well as Km data from different species.

One of the interesting observations of our study was that SULT abundance was higher in the intestines than in the livers in rodents, which is completely the opposite in humans. These findings indicate key physiologic differences regarding the need of SULT for the metabolism of endobiotics. Further investigations are needed to understand the evolutionary reason for these findings. UGT abundance data across tissues and across species provide new information, but caution should be taken when using these data in animal-to-human scaling. For example, UGT2B4 in humans is similar to UGT2B19 and UGT2B30 in nonhuman primates, and human UGT2B15 is similar in protein sequence to UGT2B20 and UGT2B31 in rhesus monkeys and dogs, respectively.

In conclusion, comprehensive quantitative information on non-CYP DMEs across preclinical species, including nonhuman primates (cynomolgus and rhesus monkey), dogs, rats (Sprague Dawley and Wistar Han), and mice, is presented and compared with the human data. This quantitative information on protein abundance of non-CYP DMEs will be useful in 1) extrapolation of drug metabolism data from preclinical species to humans, 2) prediction of species-specific drug tissue disposition, and 3) integration of protein abundance data with enzyme affinity to mechanistically explain the PK and disposition profiles in animal species based on the in vitro studies.

Acknowledgments

The authors would like to thank Matthew Karasu (WSU, Spokane, WA) and Dr. Mike Zientek (Takeda California, San Diego, CA) for their technical support in the sample analysis and insightful suggestions on the manuscript, respectively.

Authorship Contributions

Participated in research design: Basit, Fan, Khojasteh, Murray, Smith, Heyward, Prasad.

Conducted experiments: Basit.

Contributed new reagents or analytic tools: Heyward.

Performed data analysis: Basit, Prasad.

Wrote or contributed to the writing of the manuscript: Basit, Fan, Khojasteh, Murray, Smith, Prasad.

References

Ahire DS, Basit A, Karasu M, and Prasad B (2021) Ultrasensitive Quantification of Drug-metabolizing Enzymes and Transporters in Small Sample Volume by Microflow LC-MS/MS. *J Pharm Sci* **110**:2833–2840.

Attarwala H (2010) TGN1412: From Discovery to Disaster. *J Young Pharm* **2**:332–336.

Barré-Sinoussi F and Montagutelli X (2015) Animal models are essential to biological research: issues and perspectives. *Future Sci OA* **1**:1–3.

Basit A, Neradugomma NK, Wolford C, Fan PW, Murray B, Takahashi RH, Khojasteh SC, Smith BJ, Heyward S, Totah RA et al. (2020) Characterization of Differential Tissue Abundance of Major Non-CYP Enzymes in Human. *Mol Pharm* **17**:4114–4124.

Basit A, Radi Z, Vaidya VS, Karasu M, and Prasad B (2019) Kidney Cortical Transporter Expression across Species Using Quantitative Proteomics. *Drug Metab Dispos* **47**:802–808.

Bhatt DK and Prasad B (2018) Critical Issues and Optimized Practices in Quantification of Protein Abundance Level to Determine Interindividual Variability in DMET Proteins by LC-MS/MS Proteomics. *Clin Pharmacol Ther* **103**:619–630.

Di L (2019) The Impact of Carboxylesterases in Drug Metabolism and Pharmacokinetics. *Curr Drug Metab* **20**:91–102.

Diamond S, Boer J, Maduskuie Jr TP, Falahatpisheh N, Li Y, and Yeleswaram S (2010) Species-specific metabolism of SGX523 by aldehyde oxidase and the toxicological implications. *Drug Metab Dispos* **38**:1277–1285.

Diao X and Huestis MA (2019) New Synthetic Cannabinoids Metabolism and Strategies to Best Identify Optimal Marker Metabolites. *Front Chem* **7**:1–15.

Glaenzel U, Jin Y, Hansen R, Schroer K, Rahmanzadeh G, Pfaar U, Jaap van Lier J, Borell H, Meissner A, Camenisch G, et al. (2020) Absorption, Distribution, Metabolism, and Excretion of Capmatinib (INC280) in Healthy Male Volunteers and In Vitro Aldehyde Oxidase Phenotyping of the Major Metabolite. *Drug Metab Dispos* **48**:873–885.

Hammer H, Schmidt F, Marx-Stoelting P, Pötz O, and Braeuning A (2021) Cross-species analysis of hepatic cytochrome P450 and transport protein expression. *Arch Toxicol* **95**:117–133.

Hanioka N, Saito K, Isobe T, Ohkawara S, Jinno H, and Tanaka-Kagawa T (2021) Favipiravir biotransformation in liver cytosol: Species and sex differences in humans, monkeys, rats, and mice. *Biopharm Drug Dispos* **42**:218–225.

Lolkema MP, Bohets HH, Arkenau HT, Lampo A, Barale E, de Jonge MJA, van Doorn L, Hellemans P, de Bono JS, and Eskens FALM (2015) The c-Met Tyrosine Kinase Inhibitor JNJ-38877605 Causes Renal Toxicity through Species-Specific Insoluble Metabolite Formation. *Clin Cancer Res* **21**:2297–2304.

Manevski N, King L, Pitt WR, Lecomte F, and Toselli F (2019) Metabolism by Aldehyde Oxidase: Drug Design and Complementary Approaches to Challenges in Drug Discovery. *J Med Chem* **62**:10955–10994.

Parvez MM, Basit A, Jariwala PB, Gáborik Z, Kis E, Heyward S, Redinbo MR, and Prasad B (2021) Quantitative Investigation of Irinotecan Metabolism, Transport and Gut Microbiome Activation. *Drug Metab Dispos* **49**:683–693.

Prasad B, Bhatt DK, Johnson K, Chapa R, Chu X, Salphati L, Xiao G, Lee C, Hop CECA, Mathias A, et al. (2018) Abundance of Phase 1 and 2 Drug-Metabolizing Enzymes in Alcoholic and Hepatitis C Cirrhotic Livers: A Quantitative Targeted Proteomics Study. *Drug Metab Dispos* **46**:943–952.

Semino-Mora C, Leon-Monzon M, and Dalakas MC (1997) Mitochondrial and cellular toxicity induced by fialuridine in human muscle in vitro. *Lab Invest* **76**:487–495.

Uehara S, Yoneda N, Higuchi Y, Yamazaki H, and Suemizu H (2021) Oxidative metabolism and pharmacokinetics of the EGFR inhibitor BIBX1382 in chimeric NOG-TKm30 mice transplanted with human hepatocytes. *Drug Metab Pharmacokinet* **41**:100419.

Wang L, Prasad B, Salphati L, Chu X, Gupta A, Hop CE, Evers R, and Unadkat JD (2015) Interspecies variability in expression of hepatobiliary transporters across human, dog, monkey, and rat as determined by quantitative proteomics. *Drug Metab Dispos* **43**:367–374.

Wang P, Jia Y, Wu R, Chen Z, and Yan R (2021) Human gut bacterial β-glucuronidase inhibition: An emerging approach to manage medication therapy. *Biochem Pharmacol* **190**:114566.

Wang YQ, Shang XF, Wang L, Zhang P, Zou LW, Song YQ, Hao DC, Fang SQ, Ge GB, and Tang H (2020) Interspecies variation of clopidogrel hydrolysis in liver microsomes from various mammals. *Chem Biol Interact* **315**:108871.

Zou L, Stecula A, Gupta A, Prasad B, Chien HC, Yee SW, Wang L, Unadkat JD, Stahl SH, Fenner KS, et al. (2018) Molecular Mechanisms for Species Differences in Organic Anion Transporter 1, OAT1: Implications for Renal Drug Toxicity. *Mol Pharmacol* **94**:689–699.

Address correspondence to: Dr. Bhagwat Prasad, 412 East Spokane Falls Boulevard, Spokane, WA 99202. E-mail: bhagwat.prasad@wsu.edu